JOURNAL OF SOLID STATE CHEMISTRY 77, 211–222 (1988)

Neodymium Sites in Calcium Lanthanide Hexaaluminates, Potential Laser Materials

T. GBEHI, J. THERY,* D. VIVIEN, AND R. COLLONGUES

Laboratoire de Chimie Appliquée de l'Etat Solide, CNRS UA 302, ENSCP, 11 rue Pierre et Marie Curie, 75231 Paris Cedex 05, France

AND G. DHALENNE AND A. REVCOLEVSCHI

Laboratoire de Chimie des Solides, Université de Paris Sud, 91405 Orsay Cedex, France

Received December 21, 1987

The calcium ($CaAl_{12}O_{19}$) and lanthanide ("$LnAl_{11}O_{18}$" and $LnMgAl_{11}O_{19}$ with $Ln = La_{1-\alpha}Nd_\alpha$) hexaaluminates form a full series of solid solutions labeled C*Ln*A. Pure phases are prepared by solid state reactions at high temperatures (≥1550°C); however, single crystals are obtained only when C*Ln*A contains also Mg^{2+} ions. These crystals can be grown by the melting zone techniques using an arc image furnace. The structure of C*Ln*A is of the magnetoplumbite-type, with unit cell parameters intermediate between those of the two parent compounds. When calcium is replaced by barium, there is no solid solution and a compound (B*Ln*A) with different structure is formed. This difference seems to be related to the structural difference between the two alkaline earth hexaaluminates $CaAl_{12}O_{19}$ and "$BaAl_{12}O_{19}$." Optical absorption, fluorescence, and ESR spectra of Nd^{3+} in C*Ln*A single crystals have been investigated for various starting compositions $Ca_{1-x}(La_{1-\alpha}Nd_\alpha)_xMg_xAl_{12-x}O_{19}$ and compared with those of lanthanum–neodymium hexaaluminate (LNA), which is a promising laser material. While in LNA, Nd^{3+} ions are distributed among three almost equally populated sites; in C*Ln*A only two of these sites have been shown to be occupied. Furthermore, one of the two sites, with nearly axial symmetry, is much more populated than the other one. The higher the calcium content of C*Ln*A, the higher the Nd^{3+} occupancy ratio in this axial site. The fluorescence spectra of LNA and C*Ln*A are very similar. All these results suggest that as a laser material, C*Ln*A could present some interesting particularities compared to LNA.

Introduction

The lanthanum–neodymium hexaaluminate $La_{1-\alpha}Nd_\alpha MgAl_{11}O_{19}$, hereafter referred to as LNA, is a promising laser material which could potentially replace the YAG : Nd in some of its applications (*1–4*). It has been discovered and extensively studied in this laboratory (*4–6*). Its structure, like other $LnMgAl_{11}O_{19}$ or "$LnAl_{11}O_{18}$," is related to the magnetoplumbite Pb $Fe_{12}O_{19}$ (MP) with space group $P6_3/mmc$. The unit cell is made of spinel-like blocks separated by mirror planes perpendicular to the *c* axis and containing the large lanthanide ions. According to the regular MP structure these last cations should occupy a single site with axial symmetry (D_{3h}). How-

* To whom correspondence should be addressed.

0022-4596/88 $3.00

ever in LNA, single-crystal X-ray diffraction (*5*) and optical investigations (*6*) have shown that Nd^{3+} is distributed among three different sites with C_{2v} symmetry. At present we do not know if all three sites are laser active. Therefore it would be of interest to study similar compounds in which one site is privileged with respect to the two others.

In the alkaline and alkaline earth oxides–alumina phase diagrams, there are hexagonal aluminates (with $P6_3/mmc$ space group). The compounds with theoretical formula $X^{I}Al_{11}O_{17}$ in which X^{I} stands for alkaline ion, are the well-known β aluminas (*7*). The β and MP structures are similar but the mirror planes containing the large cations are closely packed for MP and loosely packed for β. It follows that alkaline ions can move in β alumina mirror planes. The compounds with the theoretical formula $X^{II}Al_{12}O_{19}$ ($X^{II} = Ca^{2+}$, Sr^{2+}) are of the MP-type structure (*8*), while for $X^{II} = Ba^{2+}$ there are in fact two compounds labeled phases I and II (*9, 10*) with two different compositions and both structurally related to β alumina.

Furthermore, there are also mixed aluminates containing two types of large cations, with different valencies. The structure is made of an alternate stacking of β and MP half unit cells, each containing one type of large cation. It belongs to the $P\bar{6}m2$ space group. They occur in the alkaline β alumina–lanthanide hexaaluminate and barium aluminate–lanthanide aluminates systems and have been labeled respectively S*Ln*A and B*Ln*A (*11, 12*).

The present study deals with the mixed compounds between calcium hexaaluminate and lanthanide hexaaluminates (C*Ln*A). We report here the synthesis, crystal growth, and characterization of C*Ln*A for $Ln = La_{1-\alpha}Nd_{\alpha}$. The structural behavior of this phase is compared to that of B*Ln*A and the results of its spectroscopic studies are discussed with reference to LNA.

Synthesis and Characterization of C*Ln*A

(*1*) *Compounds Obtained by Solid State Reaction*

Mixed phases between $X^{II}Al_{12}O_{19}$ and "$LnAl_{11}O_{18}$" or $LnMgAl_{11}O_{19}$ ($Ln = La_{1-\alpha}Nd_{\alpha}$, $0 \leq \alpha \leq 1$) have been synthesized for $X^{II} = Ca^{2+}$ and Sr^{2+}, but the present paper will be concerned only with the compounds obtained for $X^{II} = Ca^{2+}$, hereafter referred to as C*Ln*A or $Ca_{1-x}Ln_x$ to emphasize the lanthanide–calcium ratio of a particular phase.

C*Ln*A compounds, with the general formula $Ca_{1-x}Ln_xAl_{12-x}O_{19-x}$ or $Ca_{1-x}Ln_xMg_xAl_{12-x}O_{19}$ are obtained by heating at high temperatures a mixture of the following starting materials in the appropriate amounts: $CaCO_3$, Ln_2O_3, α-Al_2O_3, and eventually MgO. About 2 g of an intimate mixture of the starting compounds are cold pressed and the pellets prereacted by heating at 1200°C in air for 2 days. The samples are crushed, pressed again, and annealed for 2 days at 1550°C or 15 hr at 1600°C.

For all values of x, the X-ray powder patterns of C*Ln*A compounds contain diffraction lines characteristic of β or MP only, whose patterns exhibit $00l$ and hhl lines with l always even (Fig. 1). This behavior is different from those of S*Ln*A and B*Ln*A which exhibit also $00l$ and hhl lines with l odd. Such lines are forbidden in the β and MP $P6_3/mmc$ space group but not in the S*Ln*A $P\bar{6}m2$ space group. This indicates that in C*Ln*A all the mirror planes perpendicular to the c axis are equivalent, Ca^{2+} and Ln^{3+} ions being distributed in the same planes. This situation is different for the S*Ln*A or B*Ln*A structure in which the two types of large cations are localized in different and alternating mirror planes.

When C*Ln*A compounds are melted in a high-temperature image arc furnace, two cases must be distinguished:

—For the series $Ca_{1-x}Ln_xAl_{12-x}O_{19-x}$ the melting is incongruent, like the parent

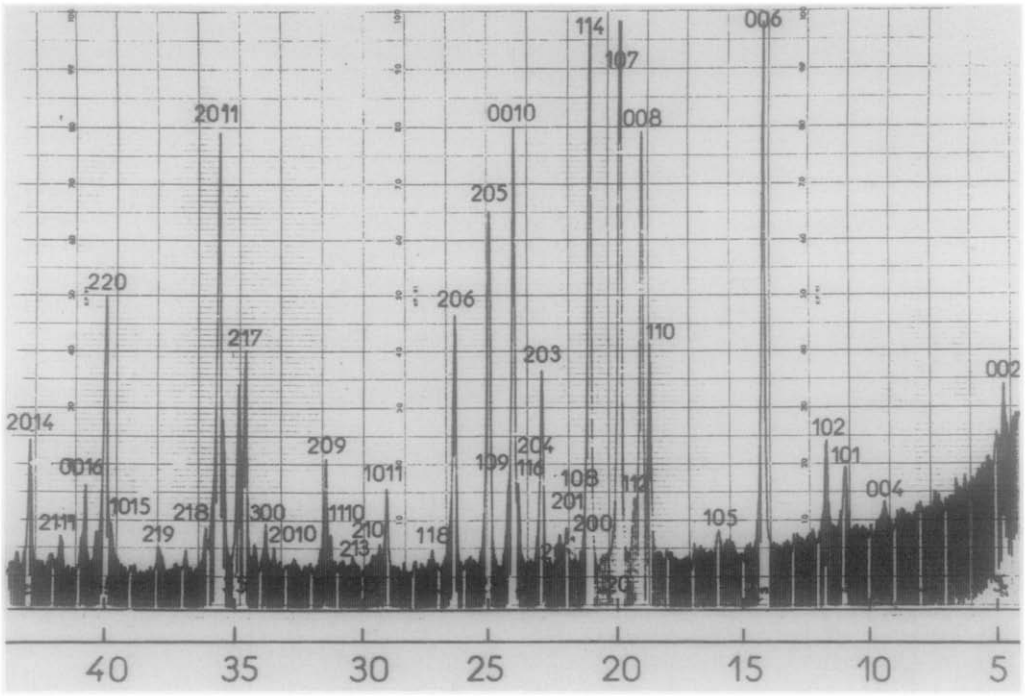

FIG. 1. X-ray powder diffraction pattern of C*Ln*A (Co*Kα* radiation) with starting composition $Ca_{0.5}Ln_{0.5}Mg_{0.5}Al_{11.5}O_{19}$.

compounds $CaAl_{12}O_{19}$ and "$LnAl_{11}O_{18}$" (*13, 14*).

—For the series $Ca_{1-x}Ln_xMg_xAl_{12-x}O_{19}$ the melting is congruent, like LNA (*5*). Crystal growth experiments have been undertaken on this second series of compounds.

(2) *Crystal Growth of CLnA by the Floating Zone Method*

C*Ln*A crystals are grown in air by the floating zone method using a focused 6.5-kW xenon arc lamp as the heat source (*15*). The crystal translation rate is chosen between 3 mm/hr and 7 mm/hr. The starting materials are identical with those used in the solid state reaction for the MgO-containing series. Before melting, samples in the form of parallelepipedic rungs are sintered at 1550°C for 24 hr.

The crystal growth of C*Ln*A is relatively easy and leads to single crystal rods 5 mm in diameter and 5 cm in length. The crystals exhibit some cracks probably due to thermal shock, but generally they are transparent and can be easily cleaved parallel to the growth axis. Transparent platelets are isolated from the crystals, and their Laue patterns indicate that they are parallel to **(a, b)** planes and that the growth axis is the **a** direction of the unit cell. The higher the neodymium content of the crystals, the deeper their purple coloration.

Electron probe microanalysis has been performed on cleavage platelets for several members of the series $Ca_{1-x}Ln_xMg_xAl_{12-x}O_{19}$ ($Ca_{1-x}Ln_x$). The results are given in Table I. It appears that there is a slight loss of calcium and magnesium oxides during the crystal growth.

The X-ray powder patterns of crushed single crystals of C*Ln*A are similar to those of sintered compounds shown in Fig. 1. Unit cell parameters determined from these

TABLE I

CHEMICAL COMPOSITIONS AND LATTICE PARAMETERS OF C*Ln*A SINGLE CRYSTALS AND PARENT COMPOUNDS (*Ln* = $La_{0.9}Nd_{0.1}$)

Starting compositions	Electron probe microanalysis	Lattice parameters			Ref.
		a (Å)	*c* (Å)	*c*/*a*	
$Ca_{0.7}Ln_{0.3}$	$Ca_{0.63}Ln_{0.32}Mg_{0.27}Al_{11.7}O_{19}$	5.57	21.92	3.94	This work
$Ca_{0.5}Ln_{0.5}$	$Ca_{0.42}Ln_{0.5}Mg_{0.45}Al_{11.58}O_{19}$	5.58	21.92	3.93	This work
$Ca_{0.4}Ln_{0.6}$	$Ca_{0.35}Ln_{0.57}Mg_{0.45}Al_{11.48}O_{19}$	5.58	21.94	3.93	This work
$Ca_{0.3}Ln_{0.7}$	$Ca_{0.24}Ln_{0.67}Mg_{0.76}Al_{11.3}O_{19}$	5.58	21.94	3.93	This work
$CaAl_{12}O_{19}$		5.56	21.89	3.94	(*22*)
$LnMgAl_{11}O_{19}$ (LNA)		5.58	21.97	3.93	(*5*)

patterns for some $Ca_{1-x}Ln_x$ compositions are gathered in Table I. These parameters are intermediate between those of the MP-type parent compounds $CaAl_{12}O_{19}$ and $LnMgAl_{11}O_{19}$. Usually for magnetoplumbite compounds the *c*/*a* ratio is close to 3.93 (*16*), while it is close to 3.99 for S*Ln*A (*17*) and to 4.03 for β aluminas (*16*). All the *c*/*a* values derived from Table I are very close to 3.93 which seems to indicate that the C*Ln*A is of magnetoplumbite type, the same as its parent compounds.

Optical Investigations of Nd^{3+} in C*Ln*A

(*1*) *Optical Absorption*

Preliminary studies at room temperature have demonstrated that the optical absorption spectra of C*Ln*A were independent of the lanthanum–neodymium ratio in these materials. Therefore this ratio has been adjusted for each particular compound in order to obtain sufficiently intense absorption bands.

The low temperature optical absorption of two single crystals with composition $Ca_{0.7}Nd_{0.3}Mg_{0.3}Al_{11.7}O_{19}$ and $Ca_{0.3}(La_{0.63}Nd_{0.07})Mg_{0.7}Al_{11.3}O_{19}$ respectively labeled ($Ca_{0.7}Ln_{0.3}$) and ($Ca_{0.3}Ln_{0.7}$) have been studied down to 4 K. The spectra were recorded on a Beckmann UV 5270 spectrometer fitted with an Oxford Instrument helium flow cryostat, in the wavelength range 200 to 1200 nm. In both cases the light beam was directed along the **c** crystal axis.

Among the 41 electronic states of the Nd^{3+} ($4f^3$) configuration, one, the $^2P_{1/2}$ level, is of special interest. Indeed the transition between the ground state $^4I_{9/2}$ and $^2P_{1/2}$ state is situated in a spectral range (~427 nm) in which it can be easily identified. Furthermore the $^2P_{1/2}$ level is not split by the crystal field ($J + 1/2 = 1$). Therefore, for each neodymium site and for the $^4I_{9/2} \rightarrow {}^2P_{1/2}$ transition at room temperature at most five lines are observed corresponding to the transition originating from the five Stark levels of $^4I_{9/2}$. Decreasing the temperature depopulates the highest $^4I_{9/2}$ Stark levels, and the number of lines in the spectrum decreases. Figure 2 depicts the evolution with temperature of the absorption spectrum of $Ca_{0.7}Nd_{0.3}$. It can be noticed that the lines situated on the long wavelength edge of the spectrum vanish as the temperature decreases. The similarity between the 30 and 4 K spectra (Figs. 2d and 2e) indicates that the depopulation process is already achieved at 30 K. At liquid helium temperature only the lowest Stark level of $^4I_{9/2}$ remains populated. It follows that only one

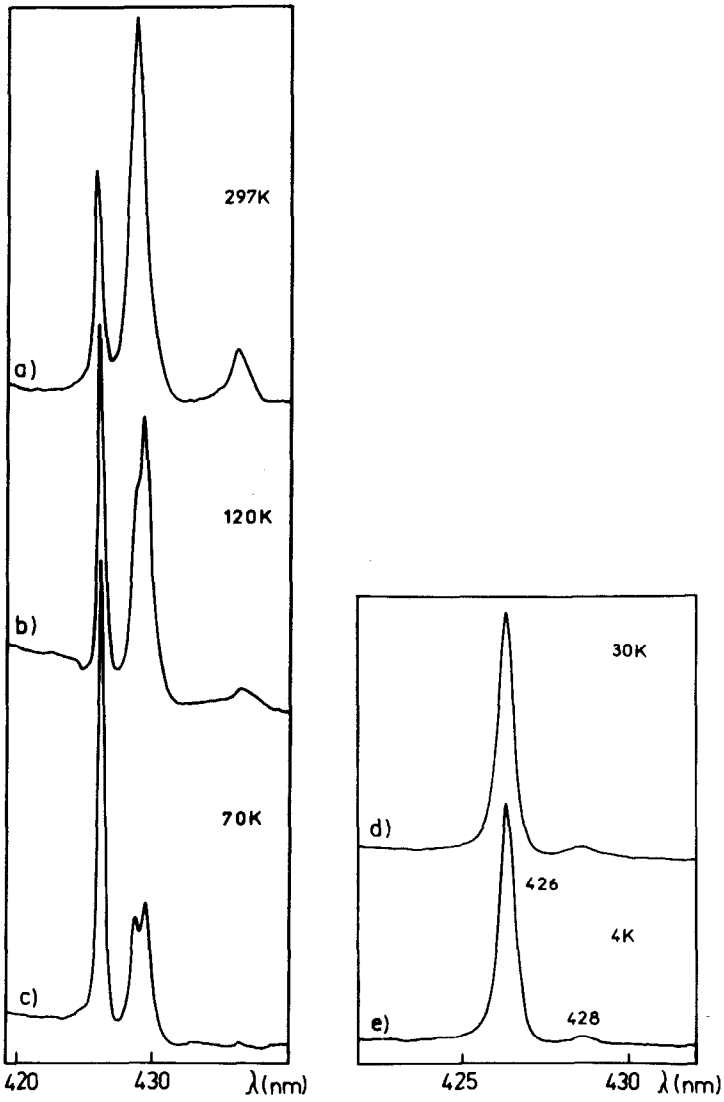

FIG. 2. Optical absorption spectra showing the temperature dependence of Nd^{3+} $^4I_{9/2} \rightarrow {}^2P_{1/2}$ transition. The C*Ln*A single crystal ($Ca_{0.7}Nd_{0.3}$) has its **c** axis along the spectrometer beam: (a) 297 K, (b) 120 K, (c) 70 K, (d) 30 K, (e) 4 K.

line is expected for the $^4I_{9/2} \rightarrow {}^2P_{1/2}$ transition of one neodymium site. Experimentally (Fig. 2e) only one strong line remains at 426 nm (labeled A line) and a much weaker one (B line) at 428 nm. Therefore in this compound Nd^{3+} is distributed among two sites, the first one corresponding to the A line being much more populated than the second.

The same procedure has already been followed for LNA (*6*), which demonstrated that in this compound neodymium is distributed among three different sites, two of which (giving a doublet) are very similar

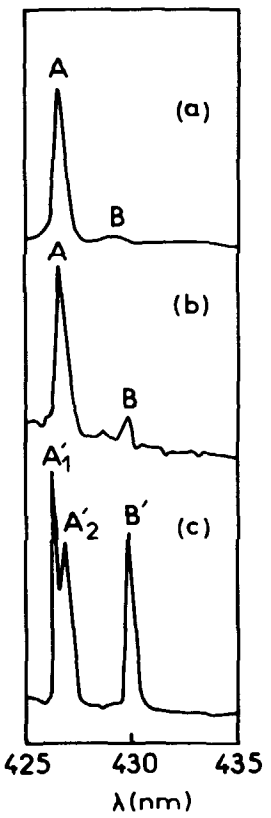

FIG. 3. Influence of the Ca/*Ln* ratio on the optical absorption spectrum of Nd^{3+} $^4I_{9/2} \rightarrow {}^2P_{1/2}$ transition at 4 K. The beam is parallel to the c axis of the crystals. Starting compositions: (a) $Ca_{0.7}Nd_{0.3}Mg_{0.3}Al_{11.7}O_{19}$ (C*Ln*A), (b) $Ca_{0.3}La_{0.67}Nd_{0.03}Mg_{0.7}Al_{11.3}O_{19}$ (C*Ln*A), (c) $La_{0.9}Nd_{0.1}MgAl_{11}O_{19}$ (LNA after (*6*)).

and the third which is rather different from the other two.

The liquid helium temperature spectra of the $^4I_{9/2} \rightarrow {}^2P_{1/2}$ transition for LNA (*6*), $Ca_{0.7}Ln_{0.3}$ and $Ca_{0.3}Ln_{0.7}$, are gathered in Fig. 3. From comparison of the three spectra it appears that the A line of C*Ln*A is in the same spectral range as the doublet (A_1', A_2') of LNA. In fact, although its wavelength is intermediate between the doublet of LNA, the linewidth at half height of the A line (~0.5 nm) is just about one-half of that of the LNA doublet. This seems to indicate that the A line is not the envelop of the LNA doublet but rather corresponds to one of its two components and therefore to a well-defined Nd site. The small shift of the C*Ln*A line compared to that of LNA may arise for instance from the difference in composition between the two compounds. Concerning the B line, it must be noticed that its intensity corresponds to 1/10 of that of the A line in $Ca_{0.7}Ln_{0.3}$, 1/5 in $Ca_{0.3}Ln_{0.7}$, and approximately 1/2 in LNA. Therefore the population of the second site increases when the calcium content of the C*Ln*A phase decreases.

A comparison of the liquid helium temperature of C*Ln*A and LNA absorption spectra can be done also for the other lines. It appears that for some transitions in which the multisite character of the neodymium in LNA is not obvious, $^4I_{9/2} \rightarrow {}^4F_{3/2}$, for instance, which contains only two lines (*6*), the spectra are identical. On the contrary, for the transitions which present in LNA more lines than allowed by the degeneracy of the state, the lines located on the long wavelength side of the LNA spectrum are always weaker or missing in C*Ln*A. This can be exemplified for the so-called hypersensitive transition $^4I_{9/2} \rightarrow {}^4G_{5/2}$, $^2G_{7/2}$ (7 lines) depicted in Fig. 4. So increasing the amount of lanthanide ions in C*Ln*A makes the spectra resemble those of LNA and populates the second neodymium site.

(2) *Neodymium Fluorescence*

The fluorescence of the C*Ln*A crystals was performed on a home-built spectrometer using a Jobin–Yvon HR 1000 monochromator and a filtered mercury arc lamp, $\lambda = 577$ nm, as excitation source. The PbS cell detector associated with a lock-in amplifier ensures the obtention of a good signal-to-noise ratio in the near infrared spectral range.

We have focused our attention on the $^4F_{3/2} \rightarrow {}^4I_{11/2}$ neodymium transition which is the most intense and corresponds to the usual

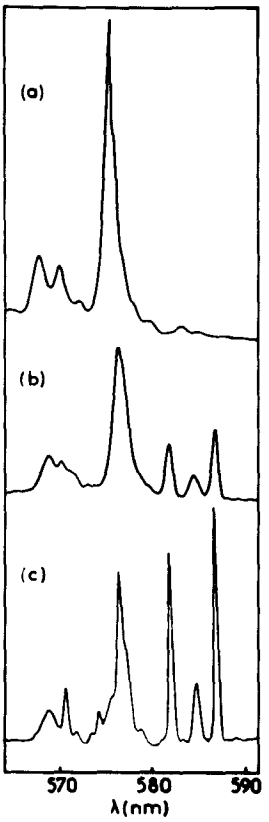

FIG. 4. Influence of the Ca/*Ln* ratio on the optical absorption spectrum of Nd^{3+} $^4I_{9/2} \rightarrow {}^4G_{5/2}$, $^4G_{3/2}$ hypersensitive transition at 4 K. The beam is parallel to the c axis of the crystals. Starting compositions: (a) $Ca_{0.7}Nd_{0.3}Mg_{0.3}Al_{11.7}O_{19}$ (C*Ln*A), (b) $Ca_{0.3}La_{0.67}Nd_{0.03}Mg_{0.7}Al_{11.3}O_{19}$ (C*Ln*A), (c) $La_{0.9}Nd_{0.1}MgAl_{11}O_{19}$ (LNA after (*6*)).

laser transition, around 1.06 μm, of Nd^{3+} activated materials. The spectra of four crystals $Ca_{1-x}Ln_x$ (x = 0.3, 0.5, 0.6, 0.7) have been recorded at room temperature. Figure 5a gives the spectrum of a $Ca_{0.7}Nd_{0.3}$ crystal which can be accurately simulated as a sum of five Gaussian shaped lines as depicted in Figure 5b. The corresponding line positions and relative intensities are given in Table II. This spectrum, like the other crystals, looks very similar to that of LNA (*1*). However, neglecting the first two weak lines whose positions are not known

TABLE II

WAVELENGTHS AND RELATIVE INTENSITIES OF THE INDIVIDUAL Nd^{3+} FLUORESCENCE LINES OF THE $^4F_{3/2} \rightarrow {}^4I_{11/2}$ TRANSITION IN $Ca_{0.7}Nd_{0.3}$ (SEE FIG. 5b)

Wavelength (nm)	1041	1046	1054	1063	1076
Relative intensity	0.03	0.06	0.36	0.17	0.38

with great accuracy, it can be noticed that the wavelengths of the lines slightly depend on the composition of the crystals. While the lines at ~1054 and 1063 nm are almost

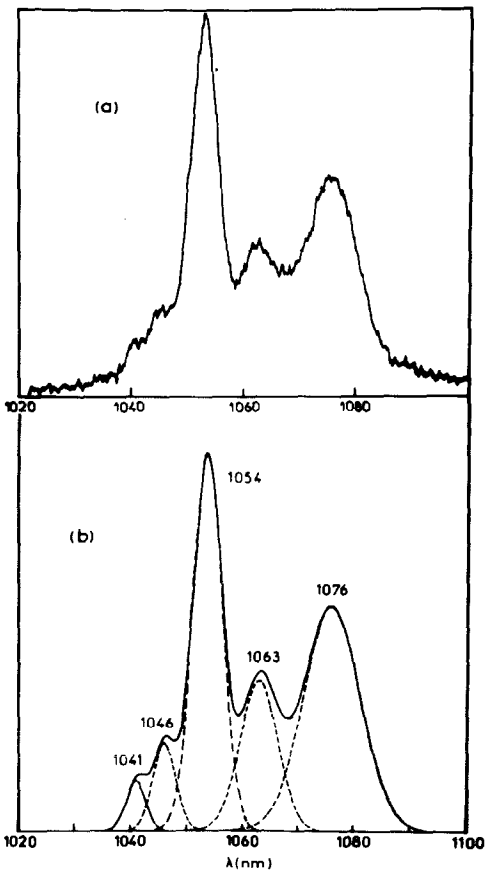

FIG. 5. Nd^{3+} fluorescence spectrum at 300 K ($^4F_{3/2} \rightarrow {}^4I_{11/2}$ transition) in C*Ln*A crystal with starting composition $Ca_{0.7}Nd_{0.3}Mg_{0.3}Al_{11.7}O_{19}$ (excitation λ = 577 nm). (a) Experimental spectrum. (b) Simulated spectrum.

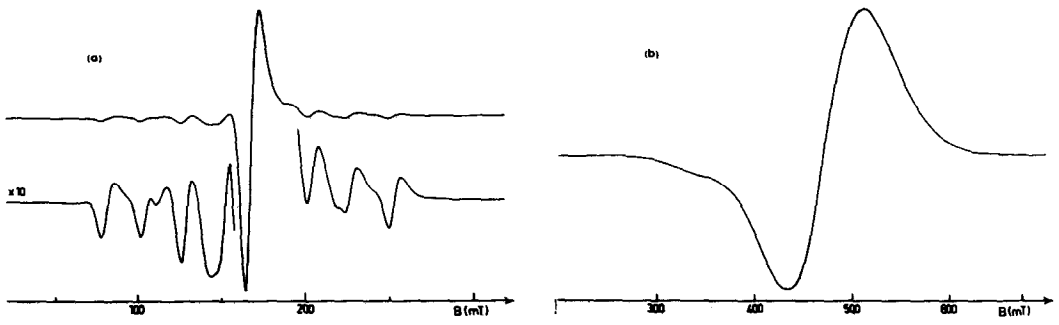

FIG. 6. 20 K ESR spectra of Nd^{3+} in single-crystalline C*Ln*A ($Ca_{0.7}La_{0.27}Nd_{0.03}Mg_{0.3}Al_{11.7}O_{19}$). (a) $B_0 \parallel \mathbf{c}$ for two values (1 and 10) of the spectrometer gain. (b) $B_0 \perp \mathbf{c}$.

insensitive to the calcium content of the crystals, the line around 1076 nm shifts toward the long wavelengths when the x value increases. For example, this line appears at ~1080 nm for $Ca_{0.3}Ln_{0.7}$. Once again when the calcium content decreases the spectrum joins that of LNA one whose main lines appear at ~1054 and 1082 nm.

ESR Investigations of Nd^{3+} in C*Ln*A

This study has been performed on single crystals of $Ca_{1-x}Ln_xMg_xAl_{12-x}O_{19}$ and only on powders of $Ca_{1-x}Ln_xAl_{12-x}O_{19-x}$ because, as already pointed out, it is not possible to grow single crystals of phases without magnesium. The neodymium content of the C*Ln*A samples was chosen so that $Ln = La_{0.9}Nd_{0.1}$. This ensures that dilution of Nd^{3+} is sufficient to prevent any magnetic interaction between neodymium centers which could broaden the ESR lines. The spectra were obtained on a Bruker ER 220 D spectrometer operating at X band, fitted with an Oxford Instrument ESR 9 helium flow cryostat. Cryogenic temperatures were required to lengthen the spin lattice relaxation time sufficiently to avoid lifetime broadening of the ESR spectra (*6*). Usually, the spectra were run at 20 K.

(*1*) *ESR of Single Crystals*

Angular variations of the ESR spectra were performed by rotating the crystal with respect to the static magnetic field B_0, in such a way that B_0 is either in a plane containing the **c** crystal direction, or in a plane perpendicular to **c** (**(a, b)** or cleavage plane).

When B_0 is along **c** the spectrum is dominated by a strong line at ~170 mT which broadens and then disappears when the temperature is raised above 50 K. This line is the narrowest (~10 mT) for this orientation, its intensity is maximum, and its field position is minimum (Fig. 6a). This indicates that **c** is one of the principal axes of the g tensor of Nd^{3+} ions which behave as an $S = 1/2$ system because at 20 K only the lowest Kramers doublet is populated. Additional hyperfine lines flanking the central line can be seen (Fig. 6a). They arise from interactions with the nuclei of the ^{143}Nd and ^{145}Nd isotopes (natural abundance 12.2 and 8.3%, respectively) both with $I = 7/2$. The ratio of the hyperfine constants associated with the two isotopes are in good agreement with the ratio of their nuclear g factors ($g_{145}/g_{143} = 0.626$).

When the magnetic field rotates from **c** to a direction of the **(a, b)** plane, the line

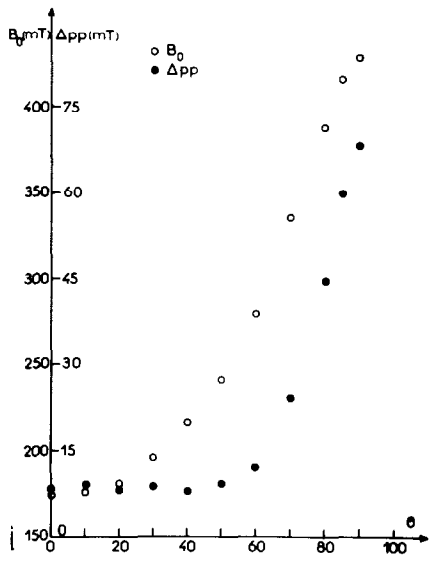

FIG. 7. Angular dependence of the ESR line position and peak-to-peak linewidth in single-crystalline C*Ln*A ($Ca_{0.7}La_{0.27}Nd_{0.03}Mg_{0.3}Al_{11.7}O_{19}$) at 20 K. The magnetic field B_0 rotates in a plane containing the **c** axis ($B_0 \parallel \mathbf{c}$ for $\theta = 0$).

moves toward higher fields and broadens markedly (Fig. 7). For B_0 perpendicular to **c** (Fig. 6b) the line reaches its higher field position (~470 mT) and its peak line width is in the range 80–100 mT.

For a rotation of B_0 in the **(a, b)** plane, the line position exhibits a very small angular dependence (amplitude ~10 mT) with a 60° periodicity. This indicates that Nd^{3+} occupies a nearly axial site, probably very close to the theoretical D_{3h} large cation site of the magnetoplumbite structure.

The experimental spin Hamiltonian parameters for the four crystals studied are gathered in Table III. One observes a very small and regular variation of these parameters with composition. The higher the lanthanide content of the phase, the closer the parallel parameters to those of LNA. Owing to the large linewidth of the perpendicular spectrum, the hyperfine satellites are not resolved. Therefore the $A_\perp$ parameter has been computed from the spectrum obtained at 60° from **c**, using the usual formula (*6*):

$$g_\theta^2 A_\theta^2 = g_\parallel^2 A_\parallel^2 \cos^2\theta + g_\perp^2 A_\perp^2 \sin^2\theta.$$

It ranges between 390×10^{-4} and 370×10^{-4} cm^{-1} for $Ca_{0.7}Ln_{0.3}$ and $Ca_{0.3}Ln_{0.7}$, respectively.

It can be seen that in C*Ln*A, the $g_\parallel/g_\perp$ ratio (~2.6) is very different from the $A_\parallel/A_\perp$ ratio (~1.2). This indicates that the wave functions of the two components of the ground state Kramers doublet contain appreciable contributions of higher energy states (*18*).

TABLE III

20 K EXPERIMENTAL SPIN HAMILTONIAN PARAMETERS OF C*Ln*A SINGLE CRYSTALS ($Ln = La_{0.9}Nd_{0.1}$)

ESR parameters	Starting compositions of crystals				
	$Ca_{0.7}Ln_{0.3}$	$Ca_{0.5}Ln_{0.5}$	$Ca_{0.4}Ln_{0.6}$	$Ca_{0.3}Ln_{0.7}$	$LnMgAl_{11}O_{19}$ (LNA)
$g_\parallel$	3.88	3.87	4.00	4.04	4.18[a] 4.04
$g_\perp$	1.58	1.55	1.49	1.43	1.28
$^{143}A_\parallel$ (10^{-4} cm^{-1})	449	455	459	465	478

Note. For comparison, the LNA parameters taken from Ref. (*6*) are also given in this table.

[a] For LNA parallel line is a doublet.

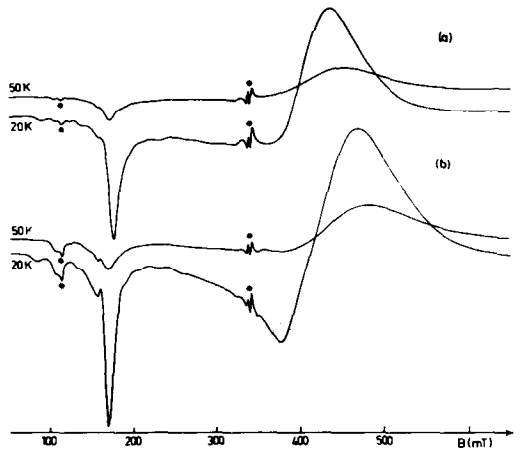

FIG. 8. Comparison of the powder ESR spectra of Nd^{3+} for two C*Ln*A compounds with starting compositions (a) $Ca_{0.5}La_{0.45}Nd_{0.05}Al_{11.5}O_{18.5}$, (b) $Ca_{0.5}La_{0.45}Nd_{0.05}Mg_{0.5}Al_{11.5}O_{19}$. Each spectrum has been recorded at 20 and 50 K. ● Denotes impurities signals. Notice that magnesium content of C*Ln*A has no influence on the spectra.

It should be mentioned for completeness that for some samples, when B_0 lies close to the **(a, b)** plane, the spectra contain additional weak features which disappear when the temperature increases above 50 K; they are ascribed to Nd^{3+} in a second site. It was not possible to obtain accurate parameters for this second Nd^{3+} spectrum. However the associated site with low occupancy ratio seems to be of low symmetry with the principal axis in the **(a, b)** plane and not along **c.**

(2) ESR of Powder Samples

In order to obtain also information concerning the neodymium localization in the magnesium-free $Ca_{1-x}Ln_xAl_{12-x}O_{19-x}$ phases, their ESR spectra were recorded and compared to those obtained on powdered crystals of C*Ln*A (containing Mg).

Figure 8 presents the powder ESR spectra of $Ca_{0.5}Ln_{0.5}Al_{11.5}O_{18.5}$ and $Ca_{0.5}Ln_{0.5}Mg_{0.5}Al_{11.5}O_{19}$ recorded at 20 and 50 K. The two spectra consist of a sharp parallel line (with hyperfine satellites) peaking at $g \sim 4$, and a broad perpendicular line crossing the baseline at $g \sim 1.6$. There are also weak impurity lines (Fig. 8) which are easily identified because, contrary to the neodymium lines, they remain sharp when the temperature goes from 20 to 50 K.

It is clear from Fig. 8 that the spectra of the two phases are identical. This indicates that, with the resolution allowed by the powder ESR spectra, the sites occupied by Nd^{3+} ions in the two series of compounds are identical.

Discussion and Conclusions

The preceding results lead us at first to compare the structure of mixed alkaline earth–lanthanide hexaaluminates according to the nature of their large divalent cation: Ca^{2+} or Ba^{2+} (C*Ln*A or B*Ln*A phases, respectively).

There is a continuous solid solution between $CaAl_{12}O_{19}$ and the lanthanide hexaaluminates ("$LnAl_{11}O_{18}$" or $LnMgAl_{11}O_{19}$, $Ln = La_{1-\alpha}Nd_\alpha$) all with magnetoplumbite-type structure. This solid solution labeled C*Ln*A belongs to the $P6_3/mmc$ space group and is also of magnetoplumbite type. Ca^{2+} and Ln^{3+} are distributed in the same (001) mirror planes, all these planes being equivalent. In contrast to this behavior, there is no solid solution between "phase I" or "phase II" barium hexaaluminates and lanthanide hexaaluminates whose structures are respectively close to β alumina and magnetoplumbite. However, in their phase diagram a new compound labeled B*Ln*A occurs in a narrow homogeneity domain (*12*). In this compound, whose structure belongs to the S*Ln*A type with $P\bar{6}m2$ space group, the (001) mirror planes are not equivalent and they are alternatively occupied by Ba^{2+} and Ln^{3+} ions. It follows that the influence of the alkaline earth ion on the behavior of the lanthanide one is more likely to occur in C*Ln*A than in B*Ln*A.

Generally speaking it appears that S*Ln*A-

type phases are formed only when one of the parent compounds is of the magnetoplumbite type and the other of the β one. This is true for alkaline–lanthanide (*17, 19*), barium–lanthanide (*12*), and also probably sodium–calcium (*20, 21*) mixed hexaaluminates. On the contrary when the two parent compounds are of the same type, they form a solid solution which belongs to the same structure. This is the case of calcium and lanthanide hexaaluminates which form C*Ln*A, a continuous series of solid solutions.

Returning to the aim of this work, one must discuss the influence of calcium on the lanthanide ions in C*Ln*A.

At first the calcium-free C*Ln*A is LNA, an interesting new laser material (*1, 4*). In this compound Nd^{3+} ions are distributed among three types of sites, corresponding to the A_1', A_2', and B′ lines of the $^4I_{9/2} \rightarrow {}^2P_{1/2}$ transition depicted in Fig. 3c. According to the relative intensity of the three lines, it could be inferred that the occupancy ratios of the three sites are rather similar. With partial substitution of calcium for lanthanide ions in LNA, the relative occupancy of the third site decreases (B lines, Figs. 3b and 3a); simultaneously one of the two first sites, responsible for the $A_1'A_2'$ doublet, disappears, the remaining Nd^{3+} site giving a strong singlet line A intermediate between A_1' and A_2'. According to its wavelength the A line originates from neodymium in high coordination (*6*) in good agreement with its quasi-axial symmetry demonstrated by ESR. This suggests a localization of neodymium in the regular large cation site of the magnetoplumbite structure with D_{3h} symmetry and 12-fold coordination. In all the samples investigated Nd^{3+} is mainly localized in this site and this is more and more true when the calcium content increases. As a consequence it will become possible to go deeper in the study of absorption spectra of LNA (*6*) by separating the contributions of the three sites which actually overlap, thus gaining a better knowledge of the local structure of LNA. However the main point is that the fluorescence spectra of C*Ln*A and LNA are very similar; therefore this fluorescence is dominated by contribution of the quasi regular Nd^{3+} site.

These results prompt us to undertake an investigation of the laser properties of this material, which finds justification in the following observations: (i) In C*Ln*A laser almost all the neodymium would contribute to the estimated emission of the material. (ii) According to the crystal growth results reported here, it seems feasible to elaborate large single-crystalline rods necessary for such a study. (iii) The neodymium dilution, which is necessary to prevent concentration quenching of fluorescence, could be achieved by varying simultaneously the lanthanum and calcium content of the material. This is one more degree of freedom with respect to LNA and could be important for optimizing laser properties.

Acknowledgments

We are indebted to Mrs. Simons, Mrs. Chatry, and Mr. Aschehoug for their technical assistance in the spectroscopic investigations.

References

1. L. D. Schearer, M. Leduc, D. Vivien, A. M. Lejus, and J. Thery, *IEEE J. Quantum Electron.* **22,** 713 (1986).
2. V. M. Garmash, A. A. Kaminskii, M. I. Polyakov, S. E. Sarkisov, and A. A. Filimonov, *Phys. Status Solidi A* **75,** K111 (1983).
3. Kh.S. Bagdasarov, L. M. Dorozhkin, L. A. Ermakova, A. M. Kevorkov, Yu.I. Krasilov, N. T. Kuznetsov, I. I. Kuratev, A. V. Potemkin, L. N. Raiskaya, P. A. Tselilin, and A. V. Shestakov, *Sov. J. Quantum Electron.* **13,** 1082 (1983).
4. D. Vivien, A. M. Lejus, J. Thery, R. Collongues, J. J. Aubert, R. Moncorge, and F. Auzel, *C. R. Acad. Sci. (Paris)* **298,** 195 (1984).

5. A. KAHN, A. M. LEJUS, M. MADSAC, J. THERY, D. VIVIEN, AND J. C. BERNIER, *J. Appl. Phys.* **52,** 6864 (1981).
6. D. SABER, J. DEXPERT-GHYS, P. CARO, A. M. LEJUS, AND D. VIVIEN, *J. Chem. Phys.* **82,** 5648 (1985).
7. R. COLLONGUES, J. THERY, AND J. P. BOILOT, *in* "Solid Electrolytes" (P. Hagenmuller and W. Van Gool, Ed.), Vol. II, p. 253, Academic Press, London (1978).
8. R. W. G. WYCKOFF, *in* "Crystal Structures," 2nd ed., Vol. III, p. 496, Wiley Interscience, New York (1965).
9. N. IYI, Z. INOUE, S. TAKEKAWA, AND S. KIMURA, *J. Solid State Chem.* **52,** 66 (1984).
10. N. IYI, Z. INOUE, S. TAKEKAWA, AND S. KIMURA, *J. Solid State Chem.* **60,** 41 (1985).
11. A. KAHN AND J. THERY, *J. Solid State Chem.* **64,** 102 (1986).
12. T. GBEHI, J. THERY, AND D. VIVIEN, *Mater. Res. Bull.* **22,** 121 (1987).
13. F. M. LEA AND C. H. DESCH, *in* "The Chemistry of Cement and Concrete," 2nd ed., p. 52, Arnold, London (1956).
14. M. ROLLIN AND P. H. THANH, *Rev. Hautes Temp. Refract.* **2,** 184 (1965).
15. A. REVCOLEVSCHI, *Rev. Int. Hautes Temp. Refract.* **7,** 73 (1970).
16. J. M. P. J. VERSTEGEN AND A. L. N. STEVELS, *J. Lumin.* **9,** 406 (1974).
17. A. RAFAOUI, A. KAHN, J. THERY, AND D. VIVIEN, *Solid State Ionics* **9–10,** 331 (1983).
18. R. J. ELLIOT AND K. W. STEVENS, *Proc. Rev. Soc. London Ser. A* **218,** 553 (1953).
19. G. AKA, J. THERY, AND D. VIVIEN, *J. Amer. Ceram. Soc.* **70,** C-179 (1987).
20. P. E. D. MORGAN, *Mater. Res. Bull.* **18,** 231 (1983).
21. P. E. D. MORGAN AND J. A. MILES, *J. Amer. Ceram. Soc.* **69,** C-157 (1986).
22. K. KATO AND H. SAALFELD, *N. Jb. Miner. Abh.* **109,** 192 (1968).